Structural Investigation of a High-Affinity Mn^{II} Binding Site in the Hammerhead Ribozyme by EPR Spectroscopy and DFT Calculations. Effects of Neomycin B on Metal-Ion Binding

Olav Schiemann,*[a] Jörg Fritscher,[a] Natalja Kisseleva,[a] Snorri Th. Sigurdsson,[b] and Thomas F. Prisner[a]

Electron paramagnetic resonance spectroscopy and density functional theory methods were used to study the structure of a single, high-affinity Mn^{II} binding site in the hammerhead ribozyme. This binding site exhibits a dissociation constant K_d of 4.4 μM in buffer solutions containing 1 M NaCl, as shown by titrations monitored by continuous wave (cw) EPR. A combination of electron spin echo envelope modulation (ESEEM) and hyperfine sublevel correlation (HYSCORE) experiments revealed that the paramagnetic manganese(II) ion in this binding site is coupled to a single nitrogen atom with a quadrupole coupling constant κ of 0.7 MHz, an asymmetry parameter η of 0.4, and an isotropic hyperfine coupling constant of $A_{iso}(^{14}N) = 2.3$ MHz. All three EPR parameters are sensitive to the arrangement of the Mn^{II} ligand sphere and can therefore be used to determine the structure of the binding site. A possible location for this binding site may be at the G10.1, A9 site found to be occupied by Mn^{II} in crystals (MacKay et al., Nature **1994**, 372, 68 and Scott et al., Science **1996**, 274, 2065). To determine whether the structure of the binding site is the same in frozen solution, we performed DFT calculations for the EPR parameters, based on the structure of the Mn^{II} site in the crystal. Computations with the BHPW91 density function in combination with a 9s7p4d basis set for the manganese(II) center and the Iglo-II basis set for all other atoms yielded values of $κ(^{14}N) = +0.80$ MHz, $η = 0.324$, and $A_{iso}(^{14}N) = +2.7$ MHz, in excellent agreement with the experimentally obtained EPR parameters, which suggests that the binding site found in the crystal and in frozen solution are the same. In addition, we demonstrated by EPR that Mn^{II} is released from this site upon binding of the aminoglycoside antibiotic neomycin B ($K_d = 1.2$ μM) to the hammerhead ribozyme. Neomycin B has previously been shown to inhibit the catalytic activity of this ribozyme (Uhlenbeck et al., Biochemistry **1995**, 34, 11186).

Introduction

Metal ions are important for the structure and function of RNA.[1] While monovalent ions can promote the folding of RNA into its secondary structure, divalent metal ions such as Mg^{II} are usually required for its folding into a biologically active tertiary structure. In addition to their structural roles, divalent metal ions have also been implicated as Lewis acid or base cofactors in the catalysis of chemical reactions by RNA.[2] Substantial knowledge about RNA – metal ion interactions has come from the study of ribozymes. A major driving force for extensive structure – function investigations on ribozymes, in addition to study of how RNA catalyzes reactions, is the fact that the catalytic activity can be used as a reporter of reaction conditions and chemical modifications. This fact has enabled chemical and biochemical experiments to probe the interactions between metal ions and RNA indirectly. The most prominent of such experiments uses phosphorothioate interference, in which the combined effects of metal ion identity and site-specific phosphorothioate substitutions on cleavage rates can give information about the coordination site(s) for specific metal ions.[3]

Most of the spectroscopic methods that have been used to study RNA – metal ion interactions utilize indirect detection. For example, fluorescence resonance energy transfer[4] and transient electric birefringence[5] can be used to study the effect of metal ions on the global conformation of RNA, but do not give any information about specific binding sites. NMR spectroscopy has also successfully been used to detect metal ion binding.[6] EPR spectroscopy of RNAs containing nitroxide spin labels has been used to extract metal ion binding constants for an isolated GAAA tetraloop[7] and to study the effects of metal ions on the structure and internal dynamics of TAR RNA.[8] However, EPR spectroscopy can also be used for the direct determination of metal ion

[a] Dr. O. Schiemann, Dipl.-Chem. J. Fritscher, Dipl.-Chem. N. Kisseleva, Prof. Dr. T. F. Prisner
Department of Physical and Theoretical Chemistry and Center for Biological Magnetic Resonance
Johann Wolfgang Goethe University
Marie-Curie-Strasse 11
60439 Frankfurt/Main (Germany)
Fax: (+49)69-79829404
E-mail: o.schiemann@prisner.de

[b] Prof. Dr. S. T. Sigurdsson
Department of Chemistry
University of Washington
Seattle, WA 98195-1700 (USA)

coordination to RNA through the replacement of Mn^{II} with the paramagnetic Mn^{II} ion. This approach has been used by DeRose and co-workers to study metal ion binding to the hammerhead ribozyme in solution (Figure 1).[9] They deduced from their
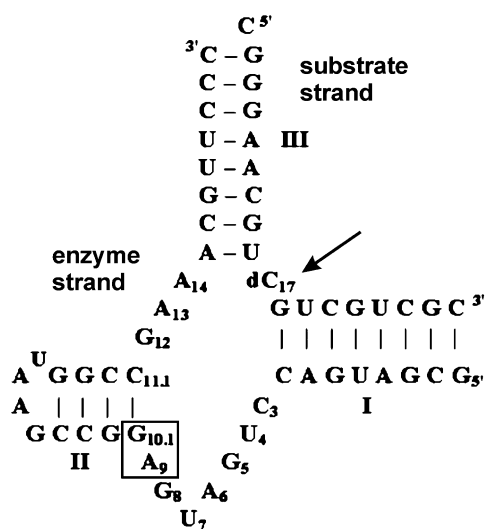

Figure 1. *Secondary structure of the hammerhead ribozyme used in our studies. The cleavage site is indicated by the arrow. The position of the Mn^{II} binding site as found in the crystal structure*[10c] *is marked by the box.*

electron spin echo envelope modulation (ESEEM)[9b] and electron nuclear double resonance (ENDOR)[9c] studies that a nitrogen and a phosphorus nucleus are located in the coordination sphere of the Mn^{II} ion and they speculate that this metal ion binding site may be situated between nucleotides A9 and G10.1 as found by X-ray crystallography.[10]

In this paper we describe the use of EPR spectroscopy and DFT calculations to show that the structure of the hammerhead A9/G10.1 metal ion binding site seems to be the same in frozen solution as in the crystal. Furthermore, we have used EPR to demonstrate that neomycin B, an aminoglycoside antibiotic that inhibits the catalytic function of the hammerhead ribozyme, displaces the essential metal ion at A9/G10.1.

Results and Discussion

Quantification of Mn^{II} binding sites

To determine the number of Mn^{II} binding sites and their relative affinities, Mn^{II} was titrated into a solution containing the hammerhead ribozyme, and the Mn^{II} signal intensity was monitored by EPR spectroscopy. In aqueous solutions, Mn^{II} forms the high-spin ($S = {}^5/_2$) [Mn(H$_2$O)$_6$]$^{2+}$ ion, which shows an intense six-line continuous wave (cw) X-band EPR spectrum at room temperature. The splitting into six lines is caused by the coupling of the electron spin to the manganese nuclear spin of $I = {}^5/_2$. However, if the Mn(II) complex is large—when it is bound to the ribozyme, for example—the rotational correlation time increases,[11] and if the Mn^{II} ion is surrounded by an asymmetric

ligand field, the zero-field splitting increases. Both effects lead to faster relaxation processes and thus to a broadening of the lines in the spectra. This line-broadening can result in nondetectability of the Mn^{II} ion at room temperature,[12] which is the case when the Mn^{II} is bound by the hammerhead ribozyme. Therefore, titration of Mn^{II} into a sample of the hammerhead ribozyme gives no signal as long as all the added Mn^{II} ions are bound by the ribozyme. When all high-affinity sites are occupied and further Mn^{II} is added, the EPR signal of the free [Mn(H$_2$O)$_6$]$^{2+}$ ion appears. The number of binding sites can hence be determined by counting the equivalents of added Mn^{II} until the EPR signal arises. Figure 2 shows such Mn^{II} titrations for three samples
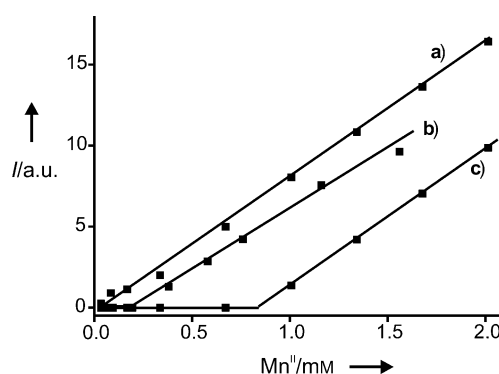

Figure 2. *Mn^{II} titration curves of samples containing a) only buffer and 1 M NaCl, b) 0.2 mM hammerhead ribozyme and 1 M NaCl, and c) 0.2 mM hammerhead ribozyme and 0.1 mM NaCl. I, doubly integrated cw EPR signal intensity of the Mn^{II} in arbitrary units (a.u.).*

containing: a) only the buffer, b) 0.2 mM ribozyme and 1 M NaCl, and c) 0.2 mM ribozyme and 0.1 M NaCl. In the presence of 0.1 M NaCl, the hammerhead ribozyme possesses four high-affinity sites (Figure 2 c), whereas a single high-affinity site is observed in the presence of 1 M NaCl (Figure 2 b). Titration of Mn^{II} into the sample without ribozyme was performed to ensure that the EPR signal of free [Mn(H$_2$O)$_6$]$^{2+}$ could be detected even at small Mn^{II} concentrations (Figure 2 a). Construction and fitting of the binding isotherms, as described in the Methods and Materials section, yielded a K_d value of 4.2 ± 1.8 μM and four independent and noncooperative binding sites with 0.1 M NaCl (Figure 3 a), and a K_d value of 4.3 ± 1.1 μM and one high-affinity binding site with 1 M NaCl (Figure 3 b). The number of binding sites and constants are in agreement with the results reported earlier by DeRose.[9a] The decrease in the number of high-affinity sites to only one at 1 M NaCl can be explained by the high ionic strength of the sodium ions at this concentration, which means that the Mn^{II} ions can only displace the sodium ions from the binding site of lowest sodium ion affinity, or that this site has the highest affinity for Mn^{II}. For the following measurements only samples with 1 M NaCl and 1 equivalent Mn^{II} were used to ensure that only one Mn^{II} site in the hammerhead ribozyme was occupied and that no free Mn^{II} was present in the sample solutions.
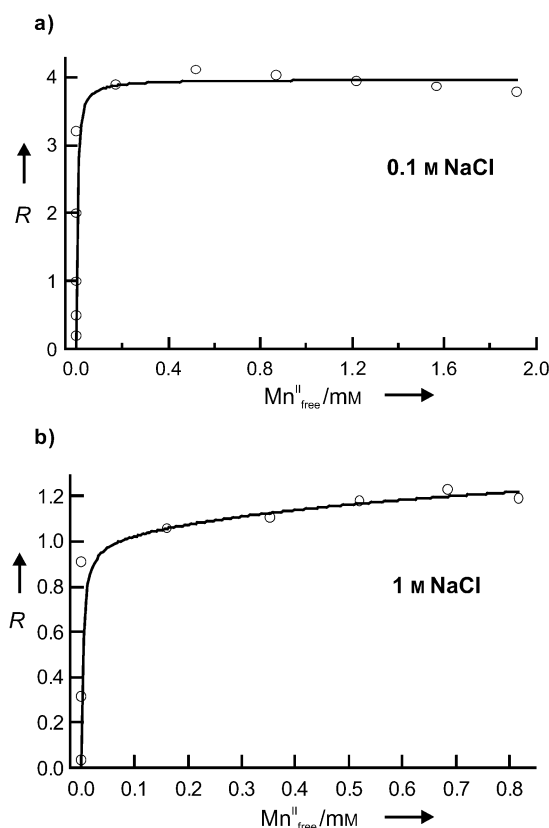
a)

0.1 M NaCl

b)

1 M NaCl

Figure 3. *Plots and fits of the Mn^{II} binding isotherms for the samples with a) 0.1 M NaCl (n = 3.99 ± 0.13 and K$_d$ = 4.2 ± 1.8 μM), and b) 1 M NaCl (n = 1.01 ± 0.19 and K$_d$ = 4.3 ± 1.1 μM). The circles in the graphs are the experimental points and the lines correspond to the respective fits by application of Equation (5). R, ratio of the concentration of bound Mn^{II} to the total concentration of ribozyme. Mn$^{II}_{free}$, concentration of free Mn^{II}.*

Pulsed EPR measurements

The spectrum of an Mn^{II} ion bound to the hammerhead can be recovered by lowering the temperature to 4 K, as a result of the longer electron spin relaxation times at this temperature. However, the cw X-band EPR spectra are still characterized by broad, inhomogeneous lines. As a result, hyperfine splittings from magnetic nuclei in the local surroundings of the manganese(II) ion are hidden by the linewidth. Therefore, pulsed EPR methods,[13] such as two-pulse and three-pulse ESEEM and HYSCORE, were employed to unravel the hyperfine and quadrupole couplings, since they contain structural information such as the distance and orientation of the ligands with respect to the metal center.[14] The corresponding pulse sequences are shown in Figure 4.

Two-pulse ESEEM

The Fourier-transformed two-pulse ESEEM spectra of the hammerhead are shown in Figure 5. Several broad and overlapping peaks can be seen in the region between 0 and 5 MHz,
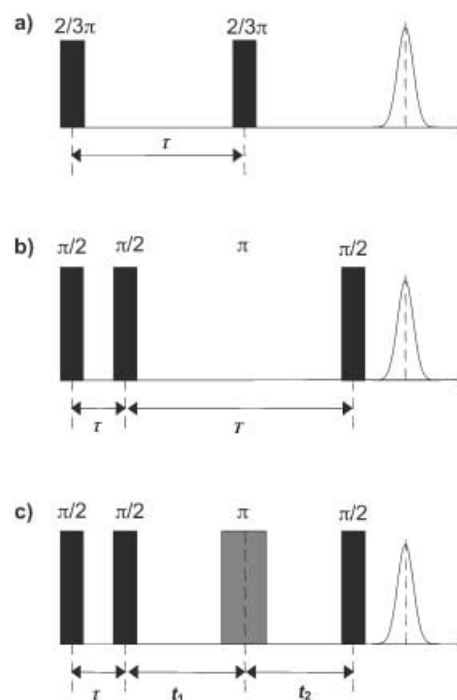
a) 2/3π ... 2/3π

b) π/2 π/2 π π/2

c) π/2 π/2 π π/2

Figure 4. *Pulse sequences of: a) two-pulse ESEEM, b) three-pulse ESEEM, and c) HYSCORE.*

^{23}Na = 4.1 MHz

B_0 = 3677 G

^{23}Na = 3.9 MHz

B_0 = 3467 G
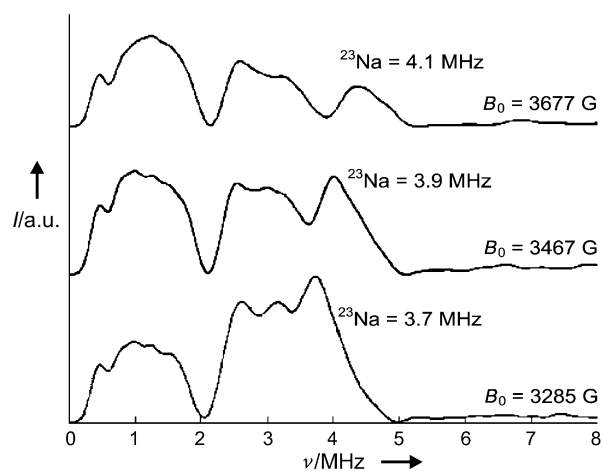
^{23}Na = 3.7 MHz

B_0 = 3285 G

Figure 5. *Fourier-transformed two-pulse ESEEM spectra at different field positions (given in the figure) of a sample with 0.2 mM ribozyme, 0.2 mM Mn^{II}, and 1 M NaCl in phosphate buffer. The other experimental parameters were: T = 4 K, pulse lengths for both pulses were 12 ns, the attenuation was set to 5 dB by use of a 1 kW TWT, τ$_{start}$ was 104 ns, the increments of τ were 8 ns, the shot repetition time was 10 ms, and 100 scans were accumulated. I, amplitude of the power Fourier transformation in arbitrary units (a.u.); ν, frequency (MHz).*

some of which may be due to sum and difference frequencies usually found in two-pulse ESEEM spectra.[13] Nevertheless, it was possible to assign one peak to weakly coupled sodium ions by monitoring its frequency shift as a function of the external magnetic field B_0 (Figure 5). At 3467 G this peak appears at 3.9 MHz, which is the free Larmor frequency of ^{23}Na at this field.

The observation that sodium ions are weakly coupled to the electron spin of Mn^{II} is not unexpected, given the high sodium concentration in the buffer. Further analysis of these spectra is hampered by the broadness of the lines, but peaks belonging to couplings of ^{14}N nuclei are generally located in this frequency region.

Three-pulse ESEEM

To obtain a better spectral resolution and to suppress sum and difference peaks, we acquired T_1-based three-pulse ESEEM spectra.[13c] To avoid blind spots in the three-pulse ESEEM spectrum, its 2D version was performed by incrementing T and τ.[13b] The Fourier-transformed spectrum in the skyline projection is shown in Figure 6. This spectrum is much better resolved than
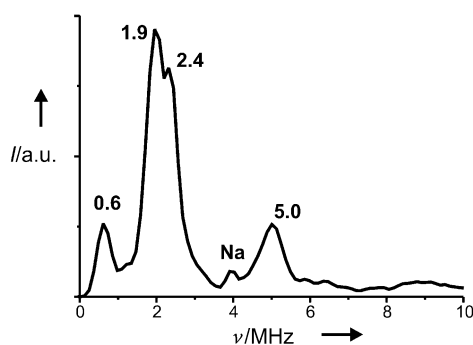

Figure 6. *Skyline projection of a 2D three-pulse ESEEM spectrum from a sample with 0.2 mM ribozyme, 0.2 mM Mn^{II}, and 1 M NaCl in phosphate buffer. The other experimental parameters were: T = 4 K, pulse lengths for all three pulses were 12 ns, the attenuation was set to 7 dB by use of a 1 kW TWT, τ_{start} was 136 ns, T$_{start}$ was 16 ns, T and τ were incremented in 8-ns steps, the dimensions of the array were 64 points by 256 points for T and τ respectively, B$_0$ = 3466 G. The shot repetition time was 10 ms, and 100 scans were accumulated. I, amplitude of the power Fourier transformation in arbitrary units (a.u.); ν, frequency.*

the two-pulse ESEEM spectra and clearly shows four peaks at 0.6, 1.9, 2.4, and 5.0 MHz. The small peak at 3.9 MHz belongs to the weakly coupled ^{23}Na ions.

To decide whether the peaks belong only to the $+ \frac{1}{2} \rightleftharpoons - \frac{1}{2}$ or to several electronic transitions, three-pulse ESEEM spectra were acquired at various microwave powers and magnetic field positions. An increase in the attenuation from 0 dB to 19 dB did not change either the frequency or the intensity ratio of the four peaks at 0.6, 1.9, 2.4, and 5.0 MHz, which should have been the case if they had belonged to different electronic transitions because of their different turning angles. However, the intensity of the peak at 3.9 MHz decreased slightly with increasing attenuation. Furthermore, on recording of the ESEEM spectra in the low-field (2767 G and 3100 G) or high-field regions (4000 G), where only the electronic $\pm \frac{1}{2} \rightleftharpoons \pm \frac{3}{2}$ and $\pm \frac{3}{2} \rightleftharpoons \pm \frac{5}{2}$ transitions contribute, none of the four peaks appeared, but only the free sodium line. All these observations together indicate that the peaks at 0.6, 1.9, 2.4, and 5.0 MHz belong to the electronic $+ \frac{1}{2} \rightleftharpoons - \frac{1}{2}$ transition, whereas the free frequency line of the sodium might originate from the $\pm \frac{1}{2} \rightleftharpoons \pm \frac{3}{2}$ or $\pm \frac{3}{2} \rightleftharpoons \pm \frac{5}{2}$ transition. The finding that the electronic $+ \frac{1}{2} \rightleftharpoons$

$- \frac{1}{2}$ transition is the major contributor to the ESEEM spectrum of Mn^{II} is in agreement with recent results from Goldfarb et al.[14]

From the finding that the four peaks belong only to the $+ \frac{1}{2} \rightleftharpoons - \frac{1}{2}$ transition, the peaks can be assigned to a nitrogen nucleus coupled to the Mn^{II} ion, which fulfills or is close to the 'exact cancellation' condition ($2\nu_N \approx A_{iso}(^{14}N)$).[13] The three peaks at 0.6, 1.9, and 2.4 MHz then belong to the ν_0, ν_+, and ν_- transitions in one electronic manifold, respectively, and the fourth peak at 5.0 MHz to the ν_{dq} transition in the other electronic manifold. The other two nuclear transitions ν_{sq1} and ν_{sq2} are usually too broad to be observed experimentally. If this assignment is correct, then the sum of the ν_0 and ν_- frequencies should give the frequency of the ν_+ transition, which is valid within the error of the experiment. Furthermore, the peak belonging to the ν_{dq} transition should be broader than the other three, which is also the case.

For a nitrogen nucleus in 'exact cancellation,' Equations (1) to (4)[13] are applicable and can be used to calculate the isotropic hyperfine coupling constant $A_{iso}(^{14}N)$, the quadrupole coupling constant $\kappa(^{14}N)$, and the asymmetry parameter of the electric field gradient tensor $\eta(^{14}N)$.

$$\nu_0 = 2\kappa\eta \tag{1}$$

$$\nu_- = \kappa(3 - \eta) \tag{2}$$

$$\nu_+ = \kappa(3 + \eta) \tag{3}$$

$$\nu_{dq} \approx 2[(\nu_N + A_{iso}/2)^2 + \kappa^2(3 + \eta^2)]^{1/2} \tag{4}$$

ν_N is the free Larmor frequency of nitrogen ^{14}N at the field position used; here ν_N(3466 G) = 1.15 MHz.

Substitution of the respective frequencies into the four equations and solving of them yields $\kappa = 0.7(1)$ MHz, $\eta = 0.4(1)$, and $A_{iso}(^{14}N) = 2.3(2)$ MHz, in agreement with values also obtained from ESEEM analysis published earlier by DeRose and Britt.[9b] Since $A_{iso}(^{14}N) = 2.3$ MHz $\approx 2\nu(^{14}N)$, it follows that the nitrogen nucleus fulfills the 'exact cancellation' condition.

Couplings to other magnetic nuclei—^{31}P, for example—could not be observed. However, this does not rule out phosphate binding to the Mn^{II} ion, since several factors can prevent the observation of a coupling in ESEEM.[9b, 9c, 15]

HYSCORE

To verify that all four peaks in the three-pulse ESEEM result from the coupling of a single nitrogen nucleus, a HYSCORE spectrum was acquired. The HYSCORE pulse sequence is depicted in Figure 4c. Incrementation of the time intervals t_1 and t_2 and Fourier transformation of the resulting time domain spectrum leads to a 2D spectrum with cross-correlation peaks in the off-diagonal region.[13b] These cross correlations are generated by the additional inversion microwave pulse (depicted in gray in Figure 4c), which transfers nuclear spin coherences from one electronic manifold to the other if they belong to the same nucleus. The HYSCORE spectrum of the Mn^{II} ion bound to the hammerhead ribozyme is shown in Figure 7. On the diagonal

there appear the same peaks as seen in the three-pulse ESEEM spectrum, and, additionally, cross correlations between all four peaks can be seen. On the basis of the simplification that the manganese(II)/nitrogen system can be treated as a $S = ^1/_2$, $I = 1$
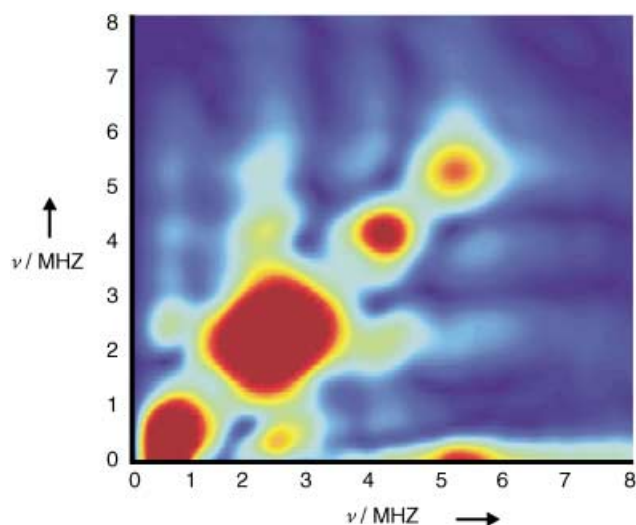

Figure 7. *The $(+, +)$ quadrant of the HYSCORE spectrum of the Mn^{II} high-affinity binding site in the region of the nitrogen couplings, recorded on a sample with 0.2 mM ribozyme, 0.2 mM Mn^{II}, and 1 M NaCl in phosphate buffer. The other experimental parameters were: T = 4 K, the pulse lengths for the three π/two-pulses were 12 ns and for the inversion pulse 24 ns, τ_{start} was 204 ns, $t_{1,start}$ was 16 ns, $t_{2,start}$ was 28 ns, and t_1 and t_2 were incremented in 8-ns steps, the dimensions of the array were 200 points by 200 points for t_1 and t_2, respectively, B$_0$ = 3466 G. The shot repetition time was 8 ms, and 70 scans were accumulated. ν, frequency in MHz.*

system, we concluded that the four peaks belong to transitions of a single nitrogen nucleus. The possibility of several magnetically equivalent nitrogen nuclei giving rise to the four peaks seems unlikely, because no combination peaks could be seen in the three-pulse ESEEM or HYSCORE spectrum.[16] It also seems unlikely that two or more nitrogen nuclei in the neighborhood of the Mn^{II} ion should be in identical environments.

Two things, however, should be mentioned. Firstly, the diagonal peaks are much more intense than for spin systems with $S = ^1/_2$. The reasons for this are the different turning angles of the electronic transitions in the $S = ^5/_2$ system and the broad spectral range, which prevented a complete inversion of the stimulated echo.[14] Secondly, it is surprising to notice that the peak at 3.9 MHz also appears to be correlated to the other four peaks on the diagonal. The cause for this remains unclear, but simulations of the HYSCORE spectrum that take all electronic transitions into account may identify the origin of these additional correlations.[14]

DFT calculations

The Mn^{II} ion in the A9,G10.1 site in the crystal structure is also bound to a single nitrogen atom belonging to guanine G10.1. Hence, to determine whether the metal ion binding site studied by EPR spectroscopy is the same site as observed in the crystal structure, we calculated the hyperfine and quadrupole coupling

parameters of the crystal structure binding site and compared them with the measured values.

Atomic coordinates from the crystal structure with a resolution of 3.00 Å reported by Scott et al.[10c] were used to construct an Mn^{II} binding site for the calculations. Water molecules were added as ligands to the vacant coordination sites of the manganese and hydrogen atoms to the open valences of all atoms, except for the phosphate groups, which carry a negative charge. This large structure was partially geometry optimized on the UHF/3-21G level. The resulting geometry and the optimized atom positions are shown in Figure 8a. This model of the
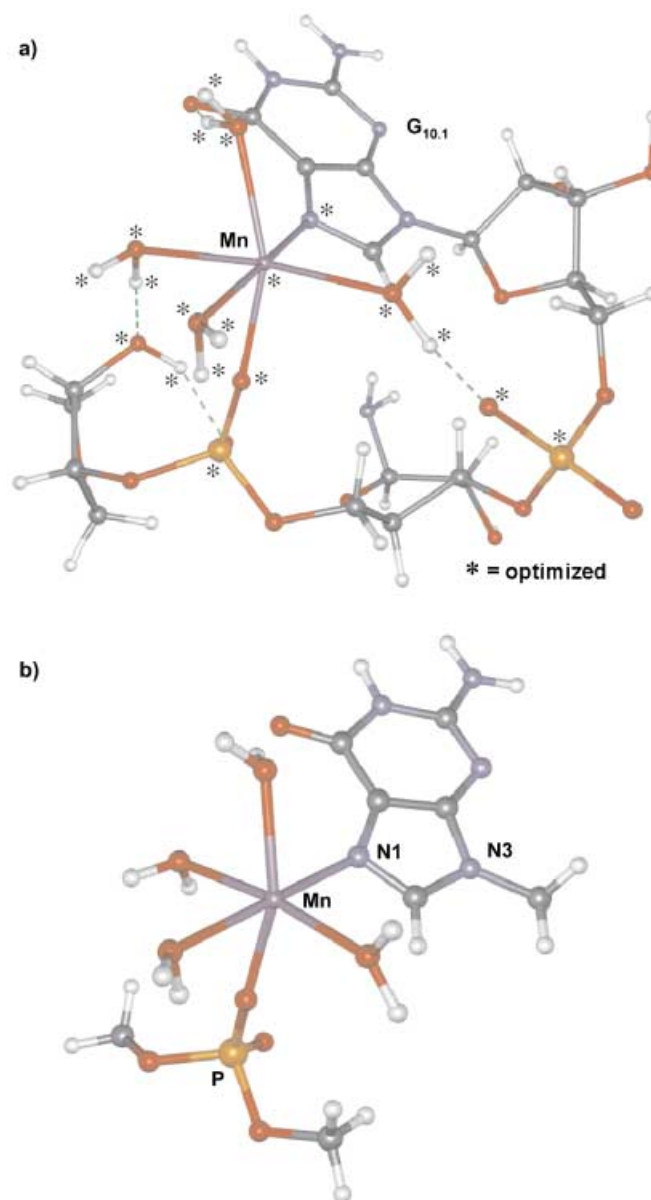

Figure 8. *a) Partially geometry-optimized (UHF/3 – 21G) large model of the Mn^{II} binding site based on the crystal structure.[10c] Water ligands were added to the open coordination sites of the manganese(II) ion and hydrogen atoms were included to saturate valences where necessary. Optimized atoms are marked by an asterisk; all other atoms were kept fixed. b) Reduced structure of the geometry-optimized model of the Mn^{II} binding site, as used for the EPR parameter calculations.*

binding site was further reduced to that shown in Figure 8b for the computation of the EPR properties, keeping only those atoms from the optimized large model that were considered as important for the magnetic properties. No additional geometry optimizations were performed for this smaller model. The reduction in size was necessary to enable large and flexible basis sets capable of accurately describing hyperfine and quadrupole properties to be applied.

For the computation of EPR properties, several density functionals were compared, and the results are shown in Table 1 together with the corresponding experimentally determined

Table 1. *Comparison of experimentally determined EPR parameters and corresponding calculated values as obtained by the use of various density functionals in combination with the 9s7p4d basis set for the Mn^{II} center and the Iglo-II basis set for all other atoms.*[a]

Method	$A_{iso}(^{55}Mn)$	$A_{iso}(^{31}P)$	$A_{iso}(^{14}N1)$	$\kappa(^{14}N1)$	$\eta(^{14}N1)$	$\langle S^2 \rangle$
BP86	−140.6	+11.6	+3.7	+0.70	0.453	8.754
BPW91	−148.6	+11.3	+3.6	+0.70	0.476	8.755
B3LYP	−154.5	+9.9	+3.9	+0.77	0.362	8.753
B3PW91	−179.5	+9.5	+3.2	+0.75	0.398	8.754
BHPW91	−228.1	+7.8	+2.7	+0.80	0.324	8.753
Exp.	255(3)	≈4[9c]	2.3(2)	0.7(1)	0.4(1)	-

[a] Expectation values of S^2 are shown in the last column. All hyperfine and quadrupole coupling constants are in MHz.

values. It can also be seen from Table 1 that spin contamination is negligible in all cases, which means that the unrestricted Kohn–Sham determinant is almost a pure spin state and does not contain admixtures from higher spin states. The results of the calculations reveal a strong influence of the choice of functional on the isotropic hyperfine coupling constant of the Mn^{II} ion. On going from BP86 to BHPW91, the Mn^{II} coupling varies by over 60%. This large effect for Mn is due to the increasing admixture of Hartree–Fock exchange, which leads to an increase of spin polarization effects and thus to an increase of negative spin density at the manganese nucleus and a larger negative isotropic hyperfine coupling constant. Such polarization mechanisms are especially important for paramagnetic metal centers in which the unpaired electrons are mainly located in *d*-type orbitals, as in high-spin Mn^{II}.[17] The BHPW91 functional containing 50% exact exchange therefore yields a value for the isotropic Mn^{II} hyperfine coupling constant $A_{iso}(^{55}Mn)$ that comes closest to experimentally determined values for Mn^{II} complexes, which usually lie in the range around (−)250 MHz. As this functional gives the best description of the spin density around the Mn^{II} ion, the results from the BHPW91 computations were used for further comparison with experimental data for the hammerhead ribozyme. A comparison of BP86 and BPW91 or B3LYP and B3PW91 shows that the PW91 correlation potential is more suitable for calculation of the isotropic Mn hyperfine coupling. In contrast to the $A_{iso}(^{55}Mn)$ hyperfine coupling, the ^{14}N hyperfine and quadrupole parameters are less strongly altered by the

different functionals and lie well within the experimental error ranges for all methods used.

Comparison of the computed values with experimental data from this work and ref. [9c] shows good agreement for both the Mn and the ligand interactions. The isotropic ^{31}P coupling is slightly overestimated, but the $^{14}N1$ parameters come very close to the experimentally determined values. This excellent agreement between the calculated and the experimentally determined hyperfine and quadrupole parameters of the nitrogen N1, which are very sensitive to geometrical changes, suggests that the binding site occupied in the crystal is also occupied in solution. In addition, these calculations support the assignment of the four peaks in the three-pulse ESEEM and HYSCORE spectra and justify the assumption of the 'exact cancellation' condition as the computed $A_{iso}(^{14}N1) = 2.7$ MHz ≈ $2\nu_N = 2.2$ MHz.

Effect of neomycin B

Neomycin B is an aminoglycoside antibiotic that inhibits hammerhead ribozyme substrate cleavage.[18] Molecular modeling studies by Westhof et al.[19] suggested that this effect may be due to the replacement of Mn^{II} by ammonium groups from neomycin B. To verify that the binding of neomycin B leads to the displacement of Mn^{II} from the binding site, a sample containing the hammerhead ribozyme with the single binding site occupied by Mn^{II}, which gives no signal in the cw EPR spectrum at room temperature, was titrated with neomycin B. As can be seen in Figure 9a, the Mn^{II} signal appears immediately and increases until saturation occurs at 1 equivalent neomycin B. Construction of the binding isotherm and fitting of the curve with the model described in the Methods and Materials section yielded a single high-affinity binding site for neomycin B with a K_d value of 1.2 ± 0.9 µM (Figure 9b). Uhlenbeck et al. determined a K_d value of 1.5 µM by monitoring the inhibition of hammerhead cleavage with respect to the neomycin B concentration.[18b]

Since the intensity and shape of the cw Mn^{II} EPR signal in the presence of the ribozyme and neomycin B resembles that of free Mn^{II}, we conclude that the Mn^{II} ion is released from its binding site by neomycin B binding to the ribozyme. To support this interpretation further, we performed a three-pulse ESEEM experiment. If the Mn^{II} ion is no longer bound in this site, then the three-pulse ESEEM spectrum should not show the peaks belonging to the coupling of the nitrogen, but may show a strong peak at the free sodium frequency due to couplings to randomly distributed sodium ions. Essentially, this is what can be seen in Figure 10. The sodium peak is visible at 3.9 MHz, now the strongest peak in the spectrum, and the characteristic four peaks of the nitrogen coupling are not observable. The peak centered at 2 MHz most probably originates from a small fraction of Mn^{II} ions still bound to the hammerhead and hence to a nitrogen atom coupling to the Mn^{II} ion ribozyme. Indeed, the cw EPR measurements showed that about 7% of the Mn^{II} was still bound to the ribozyme.

From molecular modeling and molecular dynamics simulations, Westhof et al. suggested that this release of the Mn^{II} ion may be induced because neomycin B now occupies this binding site with one of its positively charged ammonium groups.[19]
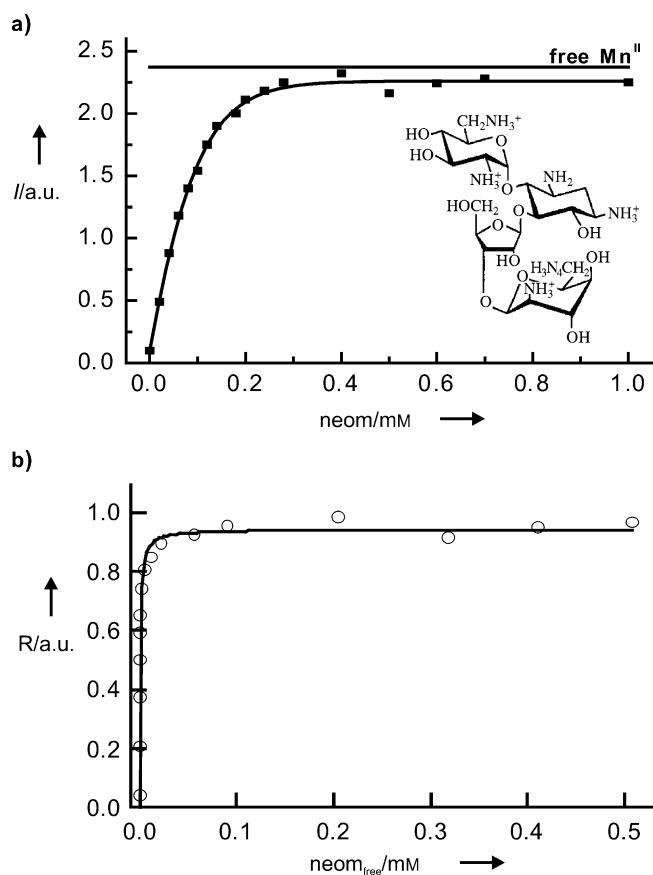
Figure 9. *a) Curve of the titration of the hammerhead ribozyme with neomycin B. The sample contained 0.2 mM hammerhead ribozyme, 0.2 mM Mn^II, and 1 M NaCl in 0.1 M phosphate buffer. The horizontal line indicates the signal intensity of free Mn^II at a concentration of 0.2 mM. I, double-integrated signal intensity of the cw EPR signal of Mn^II in arbitrary units (a.u.); neom, concentration of neomycin B in the sample. b) Plot and fit of the binding isotherm of neomycin B. The open circles are the experimental points and the line corresponds to the fit by application of Equation (5). The resulting values for the number of binding sites n and the dissociation constant K_d are n = 0.93 ± 0.09 and K_d = 1.2 ± 0.9 μM. R, ratio of bound neomycin B to the total concentration of ribozyme. neom_free, concentration of free neomycin B.*
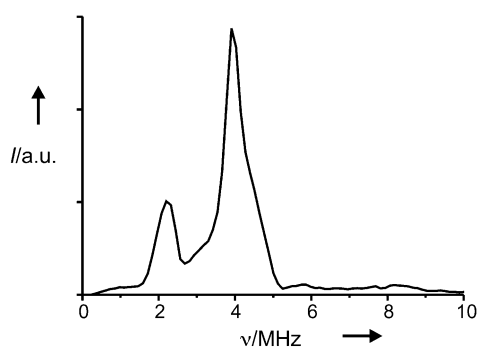

Figure 10. *Skyline projection of a 2D three-pulse ESEEM spectrum from a sample with 0.2 mM ribozyme, 0.2 mM Mn^II, 0.4 mM neomycin B, and 1 M NaCl in phosphate buffer. The other experimental parameters were: T = 4 K, pulse lengths for all three pulses were 12 ns, τ_start was 136 ns, T_start was 16 ns, T and τ were incremented in 8-ns steps, the dimensions of the array were 64 points by 256 points for T and τ, respectively, B_0 = 3466 G. The shot repetition time was 10 ms, and 100 scans were accumulated. I, amplitude of the power Fourier transformation in arbitrary units (a.u.); ν, frequency.*

Conclusion

In summary, the cw EPR titration experiments have shown that the hammerhead ribozyme possesses a single high-affinity binding site with a K_d value of 4.3 μM at a salt concentration of 1 M NaCl. Furthermore, we were able to collect information about the local surroundings of the manganese(II) ion in this binding site by using three-pulse ESEEM and HYSCORE experiments. Both experiments together revealed that the manganese(II) ion in this binding site is coupled to a single nitrogen atom exhibiting a quadrupole coupling constant κ of 0.7 MHz, an asymmetry parameter η of 0.4, and an isotropic hyperfine coupling constant of $A_{iso}(^{14}N) = 2.3$ MHz. To decide whether the same sites are occupied in the crystal and in frozen solution, we performed DFT calculations for the EPR parameters, based on the structure of the A9,G10.1 crystal binding site. The computation of the EPR parameters yielded values of $\kappa(^{14}N) = +0.80$ MHz, $\eta = 0.324$, and $A_{iso}(^{14}N) = +2.7$ MHz, in very good agreement with the experimentally obtained EPR parameters. We therefore suggest that the binding sites found in the crystal and in frozen solution are the same. In addition, we showed in a direct way, by use of cw and pulsed EPR, that the Mn^II ion is released from this site upon binding of neomycin B ($K_d = 1.2$ μM). Westhof et al. suggested that this release of the Mn^II ion may be induced because neomycin B now occupies this binding site with one of its positively charged ammonium groups.[19]

Methods and Materials

Computational details: All DFT calculations were carried out within the unrestricted Kohn–Sham formalism as implemented in the GAUSSIAN 98 program package.[20] For the partial geometry optimizations of the large structural model (see Figure 8a), the unrestricted Hartree–Fock method was used in combination with the standard basis set 3–21G. For the EPR property calculations performed with the small structural model (see Figure 8b) we compared five different combinations of exchange and correlation potentials, abbreviated as BP86, BPW91, B3LYP, B3PW91, and BHPW91. The first two consist of Becke's GGA functional for exchange (B)[21] and two different GGAs for correlation (P86[22] and PW91[23]). The third and fourth combinations use Becke's three-parameter hybrid functional (B3; includes ca. 20% exact exchange)[24] for the exchange part, and LYP[25] and PW91[23] for the correlation part. In the last case, the "half-and-half" hybrid functional (BH), which contains as much as 50% exact exchange, was used.[26]

In all computations of the hyperfine or quadrupole coupling tensors we used the 9s7p4d basis set specially developed for the calculation of ^{55}Mn hyperfine couplings by Kaupp et al.[17a] for Mn and the Iglo-II basis set[17b] for all other atoms.

CW EPR: CW X-band EPR spectra were recorded on a Bruker ESP300e EPR spectrometer, equipped with a rectangular TE_{102} resonator. Titrations of the hammerhead ribozyme with Mn^II or neomycin B were performed at room temperature in a sterilized flat cell with a volume of 200 μL. The resulting Mn^II EPR signals were base-line corrected and doubly integrated, and the magnitude of the integral was plotted against the concentration of added Mn^II. Binding isotherms for Mn^II were constructed by plotting the concentration of bound Mn^II divided by the concentration of ribozyme in solution ([Mn^II_{bound}]/[ribozyme]) versus the concentration of free Mn^II

([Mn$_{free}^{II}$]).[10a] The concentration of bound Mn^{II} was determined by comparison of the signal intensities of a Mn^{II}-ribozyme sample with a Mn^{II} standard sample containing 0.2 mM Mn^{II}, the difference in intensity between both being assigned to bound Mn^{II}. The binding isotherms were then fitted according to Equation (5) by assuming j classes of n independent non-interacting binding sites to determine the dissociation constants K_d.[27]

$$\frac{[Mn_{bound}^{II}]}{[ribozyme]} = \sum_{i=1}^{j} \frac{n_l[Mn_{free}^{II}]}{K_{d(i)} + [Mn_{free}^{II}]} \tag{5}$$

The binding isotherm of neomycin B was constructed by plotting the concentration of bound neomycin B divided by the concentration of the ribozyme versus the concentration of free neomycin B. Since one neomycin B is necessary to replace one Mn^{II}, the concentration of bound neomycin B is equal to the concentration of released Mn^{II}. The concentration of released Mn^{II} is found by comparison of the signal intensity with the intensity of the Mn^{II} standard sample. The free neomycin B is the difference between the concentration of bound neomycin B and the concentration of added neomycin B. With knowledge of the concentrations of free and bound neomycin B, the binding isotherm in Figure 9b was constructed. The number of binding sites and the K_d value were obtained by fitting of the binding isotherm according to Equation (5) and substitution of [Mn$_{free}^{II}$] by [neomycin$_{free}$] and [Mn$_{bound}^{II}$] by [neomycin$_{bound}$].

Pulsed EPR: Pulsed experiments were carried out on a Bruker ELEXSYS E580 pulsed X-band EPR spectrometer with a Bruker FT-EPR probehead and an Oxford cryostat for the temperature range from 3.8 K to 300 K. Further technical specifications are described in Ref.[28]. The pulse sequences used are shown in Figure 4. The acquired time spectra were treated in the following way: the decay was fitted exponentially and subtracted, the resulting spectrum was multiplied with a Hanning window function, zero-filling was applied, and the time domain spectrum was Fourier transformed.

Sample preparation: The ribozyme construct used[29] is depicted in Figure 1. The substrate strand was protected against cleavage by incorporation of a methoxy group at the 2′-site of the C17 sugar. The RNA was obtained gel-purified and desalted from Dharmacon. HPLC analysis showed that the strands were more than 95% pure. Autoclaved 0.1 M phosphate buffer solutions (pH 6.8) containing 0.1 M or 1 M NaCl were added to yield final ribozyme concentrations of 0.2 mM. The RNA concentrations were determined by UV/Vis by use of the extinction coefficients given in ref. [30]. For annealing of the ribozyme to the non-cleavable substrate, the following temperature program was run: 90 °C for 3 min, 60 °C for 5 min, 50 °C for 5 min, 40 °C for 5 min, and 22 °C for 15 min. A sterilized buffer solution of MnCl$_2$ (Sigma) was subsequently added. Finally, the sample was again heated to 60 °C and cooled on ice to form the tertiary structure. For the pulsed EPR measurements, aliquots (80 µL) were transferred into sterilized EPR tubes. Neomycin B was purchased from Sigma and dissolved in sterilized phosphate buffer.

Acknowledgements

[1] a) R. F. Gesteland, J. F. Atkins, *The RNA World*, Cold Spring Harbor Laboratory Press, New York, **1993**; b) D. J. Patel, *Biopolymers* **1998**, *48*, 97; c) E. V. Puglisi, J. D. Puglisi in *RNA Structure and Function* (Eds.: R. W. Simons, M. Grunberg-Manago), Cold Spring Harbor Laboratory Press, New York, **1998**, p. 117; d) F. Eckstein, D. M. Lilley (Eds.), *Nucleic Acids and Molecular Biology. Catalytic RNA*. Vol. 10, Springer, Berlin, **1997**; e) E. A. Doherty, J. A. Doudna, *Ann. Rev. Biophys. Biomol. Struc.* **2001**, *30*, 457; f) S. A. Woodson, *Cellul. Molec. Life Sci.* **2000**, *57*, 796; g) W. G. Scott, *Curr. Opin. Chem. Biol.* **1999**, *3*, 705.

[2] a) C. Hammann, D. M. Lilley, *ChemBioChem* **2002**, *3*, 690; b) M. J. Fedor, *Curr. Opin. Struct. Biol.* **2002**, *12*, 289.

[3] a) F. Eckstein, *Biochimie* **2002**, *84*, 841.

[4] a) T. Tuschl, C. Gohlke, T. M. Jovin, E. Westhof, F. Eckstein, *Science* **1994**, *266*, 785; b) G. S. Bassi, A. I. H. Murchie, F. Walter, R. M. Clegg, D. M. J. Lilley, *EMBO J.* **1997**, *16*, 7481; c) K. Bondensgaard, E. T. Mollova, A. Pardi, *Biochemistry* **2002**, *41*, 11 532; d) T. J. Wilson, D. M. Lilley, *RNA* **2002**, *8*, 587; e) N. G. Walter, K. J. Hampel, K. M. Brown, J. M. Burke, *EMBO J.* **1998**, *17*, 2378.

[5] K. M. A. Amiri, P. J. Hagermann, *Biochemistry* **1994**, *33*, 13 172.

[6] a) J. S. Summers, J. Shimko, F. L. Freedman, C. T. Badger, M. Sturgess, *J. Am. Chem. Soc.* **2002**, *124*, 14 934; b) Y. Tanaka, C. Kojima, E. H. Morita, Y. Kasai, K. Yamasaki, A. Ono, M. Kainosho, K. Taira, *J. Am. Chem. Soc.* **2002**, *124*, 4595; c) S. E. Butcher, F. H. T. Allain, J. Feigon, *Biochemistry* **2000**, *39*, 2174; d) M. R. Hansen, J. P. Simorre, P. Hanson, V. Mokler, L. Bellon, L. Beigelman, A. Pardi, *RNA* **1999**, *5*, 1099; e) M. Maderia, L. M. Hunsicker, V. J. DeRose, *Biochemistry* **2000**, *39*, 12 113.

[7] P. Z. Quin, S. E. Butcher, J. Feigon, W. L. Hubbell, *Biochemistry* **2001**, *40*, 6929.

[8] a) T. E. Edwards, T. M. Okonogi, S. T. Sigurdsson, *Chem. Biol.* **2002**, *9*, 699; b) T. E. Edwards, S. T. Sigurdsson, *Biochem. Biophys. Res. Comm.* **2003**, *303*, 721.

[9] a) T. E. Horton, D. R. Clardy, V. J. DeRose, *Biochemistry* **1998**, *37*, 18 094; b) S. R. Morrissey, T. E. Horton, C. V. Grant, C. G. Hoogstraten, R. D. Britt, V. J. DeRose, *J. Am. Chem. Soc.* **1999**, *121*, 9215; c) S. R. Morrissey, T. E. Horton, V. J. DeRose, *J. Am. Chem. Soc.* **2000**, *122*, 3473; d) T. E. Horton, V. J. DeRose, *Biochemistry* **2000**, *39*, 11 408.

[10] a) H. W. Pley, K. M. Flaherty, D. B. MacKay, *Nature* **1994**, *372*, 68; b) W. G. Scott, J. T. Finch, A. Klug, *Cell* **1995**, *81*, 991; c) W. G. Scott, J. B. Murray, J. R. P. Arnold, B. L. Stoddard, A. Klug, *Science* **1996**, *274*, 2065; PDB entry 300D.

[11] S. K. Misra, *Appl. Magn. Reson.* **1996**, *10*, 193.

[12] N. Niccolai, E. Tiezzi, G. Valensin, *Chem. Rev.* **1982**, *82*, 359.

[13] a) A. Schweiger, *Angew. Chem. Int. Ed. Engl.* **1991**, *30*, 265; *Angew. Chem.* **1991**, *103*, 223; b) A. Schweiger, G. Jeschke, *Principles of Pulsed Electron Paramagnetic Resonance*, Oxford University Press, Oxford, **2001**; c) S. A. Dikanov, Y. D. Tsvetkov, *Electron Spin Echo Envelope Modulation (ESEEM) Spectroscopy*, CRC Press, Boca Raton, **1992**.

[14] N. P. Benitis, P. C. Dave, D. Goldfarb, *J. Magn. Reson.* **2002**, *158*, 126.

[15] T. Prisner, M. Rohrer, F. MacMillan, *Annu. Rev. Phys. Chem.* **2001**, *52*, 279.

[16] Y. Deligiannakis, N. Louloudi, N. Hadjiliadis, *Coord. Chem. Rev.* **2000**, *204*, 1.

[17] a) M. Munzarová, M. Kaupp, *J. Phys. Chem. A* **1999**, *103*, 9966; b) W. Kutzelnigg, U. Fleischer, M. Schindler in *NMR—Basic Principles and Progress* (Eds.: P. Diehl, E. Fluck, H. Günther, R. Kosfeld), Springer, Heidelberg, **1990**, Vol. 23, pp. 165ff.

[18] a) T. K. Stage, K. J. Hertel, O. C. Uhlenbeck, *RNA* **1995**, *1*, 95; b) B. Clouet-d'Orval, T. K. Stage, O. C. Uhlenbeck, *Biochemistry* **1995**, *34*, 11186.

[19] T. Hermann, E. Westhof, *J. Mol. Biol.* **1998**, *276*, 903.

[20] M. J. Frisch, G. W. Trucks, H. B. Schlegel, G. E. Scuseria, M. A. Robb, J. R. Cheeseman, V. G. Zakrzewski, J. A. Montgomery Jr., R. E. Stratmann, J. C. Burant, S. Dapprich, J. M. Millam, A. D. Daniels, K. N. Kudin, M. C. Strain, O. Farkas, J. Tomasi, V. Barone, M. Cossi, R. Cammi, B. Mennucci, C. Pomelli, C. Adamo, S. Clifford, J. Ochterski, G. A. Petersson, P. Y. Ayala, Q. Cui, K. Morokuma, P. Salvador, J. J. Dannenberg, D. K. Malick, A. D. Rabuck, K. Raghavachari, J. B. Foresman, J. Cioslowski, J. V. Ortiz, A. G. Baboul, B. B. Stefanov, G. Liu, A. Liashenko, P. Piskorz, I. Komaromi, R. Gomperts, R. L. Martin, D. J. Fox, T. Keith, M. A. Al-Laham, C. Y. Peng, A. Nanayakkara, M.

Challacombe, P. M. W. Gill, B. Johnson, W. Chen, M. W. Wong, J. L. Andres, C. Gonzalez, M. Head-Gordon, E. S. Replogle, and J. A. Pople, GAUSSIAN 98 (Revision A.11), Gaussian, Inc., Pittsburgh PA, **2001**.

[21] A. D. Becke, *Phys. Rev. A* **1988**, *38*, 3098.

[22] J. P. Perdew, Y. Wang, *Phys. Rev. B* **1986**, *33*, 8822; J. P. Perdew, Y. Wang, *Phys. Rev. B* **1986**, *34*, 7406.

[23] J. P. Perdew, *Physica B* **1992**, *172*, 1; J. P. Perdew in *Electronic Structure of Solids '91* (Eds.: P. Ziesche, H. Eschring), Akademie Verlag, Berlin, **1991**; J. P. Perdew, Y. Wang, *Phys. Rev. B* **1992**, *45*, 13244.

[24] A. D. Becke, *J. Chem. Phys.* **1993**, *98*, 5648.

[25] C. Lee, W. Yang, G. R. Parr, *Phys. Rev. B* **1988**, *37*, 785; B. Miehlich, A. Savin, H. Stoll, H. Preuss, *Chem. Phys. Lett.* **1989**, *157*, 200.

[26] A. D. Becke, *J. Chem. Phys.* **1993**, *98*, 1372.

[27] I. M. Klotz, *Ligand-Receptor Energetics*, John Wiley, New York, **1997**.

[28] A. Weber, O. Schiemann, B. Bode, T. F. Prisner, *J. Magn. Res.* **2002**, *157*, 277.

[29] K. J. Hertel, D. Herschlag, O. C. Uhlenbeck, *Biochemistry* **1994**, *33*, 3374.

[30] D. M. Gray, S. H. Hung, K. H. Johnson, *Methods in Enzymology* **1995**, *246*, 19.